Genetic interactions among ADAMTS metalloproteases and basement membrane molecules in cell migration in *Caenorhabditis elegans*

Short title:

Interaction among ADAMTS proteases and basement membrane proteins

Ayaka Imanishi, Yuma Aoki, Masaki Kakehi, Shunsuke Mori, Tomomi Takano, Yukihiko Kubota, Hon-Song Kim, Yukimasa Shibata, Kiyoji Nishiwaki*

Department of Bioscience, Kwansei Gakuin University, Sanda, Japan

*To whom correspondence should be addressed:

Kiyoji Nishiwaki

Department of Bioscience, Kwansei Gakuin University

2-1 Gakuen, Sanda 669-1337, Japan

Phone: +81-79-565-7639

E-mail: nishiwaki@kwansei.ac.jp

Abstract

During development of the *Caenorhabditis elegans* gonad, the gonadal leader cells, called distal tip cells (DTCs), migrate in a U-shaped pattern to form the U-shaped gonad arms. The ADAMTS (a disintegrin and metalloprotease with thrombospondin motifs) family metalloproteases MIG-17 and GON-1 are required for correct DTC migration. Mutations in *mig-17* result in misshapen gonads due to the misdirected DTC migration, and mutations in *gon-1* result in shortened and swollen gonads due to the premature termination of DTC migration. Although the phenotypes shown by *mig-17* and *gon-1* mutants are very different from one another, mutations that result in amino acid substitutions in the same basement membrane protein genes, *emb-9/collagen IV a1*, *let-2*/*collagen IV a2* and *fbl-1/fibulin-1*, were identified as genetic suppressors of *mig-17* and *gon-1* mutants. To understand the roles shared by these two proteases, we examined the effects of the *mig-17* suppressors on *gon-1* and the effects of the *gon-1* suppressors and enhancers on *mig-17* gonadal defects. Some of the *emb-9*, *let-2* and *fbl-1* mutations suppressed both *mig-17* and *gon-1*, whereas others acted only on *mig-17* or *gon-1*. These results suggest that *mig-17* and *gon-1* have their specific functions as well as functions commonly shared between them for gonad formation. The levels of collagen IV accumulation in the DTC basement membrane were significantly higher in the *gon-1*

mutants as compared with wild type and were reduced to the wild-type levels when combined with suppressor mutations, but not with enhancer mutations, suggesting that the ability to reduce collagen IV levels is important for *gon-1* suppression.

Introduction

Members of the ADAMTS family of secreted zinc metalloproteases have important roles in animal development. Most of these proteases degrade extracellular matrix components such as proteoglycans or collagens [1]. Nineteen ADAMTS genes have been identified in the human genome, and mutations in many of them result in hereditary diseases that are related to disorders of the extracellular matrix [2, 3]. Multiple ADAMTS proteases often function in a common developmental process. For example, the functions of ADAMTS-5, -9 and -20 are required for interdigital web regression [4]. ADAMTS-9 and -20 are needed for closure of the palate and for craniofacial morphogenesis and neural tube closure through their function in ciliogenesis [4, 5]. ADAMTS-5 and -15 act in myoblast fusion [6]. These enzymes appear to function in a partially overlapping manner. However, the roles shared by these ADAMTS proteases in development still remain elusive.

Among five ADAMTS genes in *C. elegans*, *gon-1* and *mig-17* play essential roles

in the development of the somatic gonad [7, 8]. Both GON-1 and MIG-17 localize to the gonadal basement membrane (BM) [9, 10]. In the *mig-17* mutants, DTCs meander and stray, resulting in an abnormal gonadal shape. In contrast, in the *gon-1* mutants, DTCs rarely migrate and the gonads remain small. We have isolated and analyzed the genetic suppressors for DTC migration defects in *mig-17* mutants. Dominant gain-of-function mutations in the *fbl-1/fibulin-1* and *let-2/collagen IV α2* chain, which encode BM molecules, have been frequently isolated as suppressors [11, 12]. The *fbl-1(gf)* mutations are amino acid substitutions in the second epidermal growth factor–like motif of FBL-1C, one of the two splicing isoforms, and FBL-1C protein is secreted by the intestine to be released into the gonadal BM in a MIG-17 activity-dependent manner [11]. Suppression of *mig-17* by *fbl-1(gf)* mutations is dependent on the BM molecule NID-1/nidogen [12]. *let-2(gf)* mutations are associated with amino acid changes within the triple helix domain or the C-terminal non-collagenous domain (NC)1 of collagen IV. LET-2 protein is secreted from body wall muscle cells and DTCs and localized to the gonadal BM in a MIG-17 activity-independent manner. Unlike the case of *fbl-1(gf)*, suppression of mig-17 by *let-2(gf)* mutations does not require NID-1 [12].

Genetic suppressor analysis of *gon-1* mutants revealed that loss-of-function (deletion) mutations in *fbl-1* can suppress the shortened-gonad phenotype of *gon-1*

mutants. Because *fbl-1* deletion mutants also exhibit the shortened-gonad phenotype, GON-1 and FBL-1 act antagonistically to regulate gonad formation [13]. This genetic interaction is mediated by the control of collagen IV accumulation in the gonadal BM: GON-1 acts to reduce collagen IV levels, whereas FBL-1 acts to maintain collagen IV levels [14].

Although *mig-17* and *gon-1* mutants are phenotypically very different, they are both suppressed or enhanced by mutations in *let-2* and *fbl-1*. In this study, we isolated novel suppressor mutations in *emb-9* for *mig-17* and in *let-2* for *gon-1* gonadal defects. Together with the previously isolated suppressors and enhancers, we investigated the consequences when suppressors for *mig-17* were combined with *gon-1* mutations, and when *gon-1* suppressors and enhancers were combined with *mig-17* mutations. We found that some of the *emb-9*, *let-2* and *fbl-1* mutations suppressed both *mig-17* and *gon-1*, whereas others suppressed only *mig-17* or *gon-1*. These results suggest that *mig-17* and *gon-1* have their specific functions as well as the functions commonly shared between them for gonad formation.

Materials and Methods

Strains and genetic analysis

Culture, handling and ethyl methanesulfonate (EMS) mutagenesis of *C. elegans* were conducted as described [15]. The following mutations and transgenes were used in this work: *mig-17(k174)*, *gon-1(e1254, g518)*, *fbl-1(k201, tk45)*, *let-2(g25, b246, k193, k196)*, *emb-9(tk75, g34, g23cg46)* and *tkTi1[emb-9::mCherry]* [7, 8, 11, 12, 14, 16-18]. The suppressor mutations were genetically mapped with single-nucleotide polymorphism mapping using *mig-17(k174)* and *gon-1(e1254)* mutant strains, which are in the CB4856 background [19]. Among the 11 *mig-17(k174)* suppressors, *k204* and *k207* were mapped to the center of linkage group (LG) III. Next-generation sequence analysis identified missense mutations in *emb-9* in these suppressors. Of the two *gon-1(e1254)* suppressors, one was mapped to the right end of LG X and was identified by next-generation sequence analysis as corresponding to a missense mutation in *let-2*. All experiments were conducted at 20°C. The temperature-sensitive mutants *emb-9(g34)* and *let-2(g25, b246)*, which arrest during embryogenesis or early larval stages at 25°C, do proliferate at 20°C. Because *gon-1(e1254, g518)* and *fbl-1(tk45)* mutants were sterile, we used the genetic balancer *nT1[qIs51] (IV;V)* to maintain these mutants and to generate double mutants containing these mutations.

Microscopy

Gonad migration phenotypes were scored using a Nomarski microscope (Axioplan 2; Zeiss). Analysis of gonadal phenotypes was performed at the young-adult stage as described [20]. Although the gonadal phenotypes of some strains used are published, we reevaluated them in this study. The levels of EMB-9-mCherry were quantified as follows. For each sample, confocal images of a sagittal section of the DTCs were obtained with a Zeiss Imager M2 microscope equipped with a spinning-disk confocal scan head (CSU-X1; Yokogawa) and an ImageEM CCD camera (ImageEM; Hamamatsu Photonics). Using ImageJ software, we measured the fluorescence intensities along three drawn lines, each of which crossed the DTC BM; the average background intensities inside the gonad were subtracted from the peak values of the line scan, and the resulting corrected values were averaged.

Transgenic analysis of suppressors

Germline transformation was carried out as described [21]. Plasmids containing *emb-9(k204)*, *emb-9(k207)* and *let-2(tk101)* were constructed by introducing these mutations individually into their respective wild-type constructs [12, 14]. These plasmids were injected into the *unc-119(e2498)* gonad at 1–2 ng/µl with 10 ng/µl *unc-119+* plasmid [22], 70 ng/µl *sur-5::gfp* plasmid [23] and 70 ng/µl pBSIIKS(−), and

126 the resulting extrachromosomal arrays were transferred to either *mig-17(k174); unc-*
127 *119(e2498)* or *gon-1(e1254); unc-119(e2498)* animals by mating.
128
129 **Homology modeling of NC1 domains**
130 Homology modeling was conducted based on the crystal structures of bovine collagen
131 IV NC1 domains [24] using the SWISS-MODEL server. Ribbon diagrams were
132 created and edited with the Swiss-Pdb Viewer software.
133
134 ## Results
135 **Isolation of novel suppressors of *mig-17* and *gon-1* mutants**
136 The *C. elegans* hermaphrodite gonad arms extend to the anterior-right and posterior-left
137 areas of the body cavity. The U shape of the gonad arms are generated by migration of
138 the gonadal leader cells, the DTCs, over the body wall during larval development (S1
139 Fig). *gon-1* mutants exhibit shortened gonads due to the premature termination of DTC
140 migration and are sterile. In contrast, *mig-17* mutants show misshapen gonad arms due
141 to the misdirected migration of DTCs, but they are still fertile. Although both of these
142 genes encode ADAMTS family metalloproteases, the phenotypes shown by these
143 mutants are very different.

144 The null allele *gon-1(q518)* exhibits a fully penetrant short gonad phenotype that
145 cannot be distinguished from that of the *mig-17(k174)*; *gon-1(q518)* double null mutants
146 [8]. The phenotypic penetrance of *gon-1(e1254)*, a partial loss-of-function allele that
147 results in a milder gonad phenotype as compared with *gon-1(q518)*, was enhanced in
148 combination with the *mig-17(k174)* null allele (Fig 1A; S2 Fig), indicating that *gon-1*
149 and *mig-17* function in partially overlapping pathways.
150
151 **Fig 1. DTC migration phenotypes of *mig-17*, *gon-1* and the suppressors. A.**
152 Percentage of DTC migration defects in *mig-17(k174)* and *gon-1(e1254)* single mutants
153 and their double mutants. **B.** Percentage of DTC migration defects in *mig-17(k174)*
154 animals with the *emb-9(k204)* or *emb-9(k207)* mutation or with extrachromosomal
155 arrays carrying these mutant genes. **C.** Percentage of DTC migration defects in *gon-*
156 *1(e1254)* or *gon-1(q518)* animals with a *let-2(tk101)* mutation or with an
157 extrachromosomal array carrying the *let-2(tk101)* mutant gene.
158
159 To identify genes interacting with *mig-17* and *gon-1*, we isolated novel
160 suppressor mutations for DTC migration defects of *mig-17* and *gon-1* mutants using
161 EMS mutagenesis. We isolated 11 suppressor mutants of *mig-17(k174)*, a null allele that

has a nonsense mutation in the pro-domain (S2 Fig). Two of these mutants, *k204* and *k207*, were genetically mapped near the center of LG III and acted as dominant suppressors for *mig-17* (Fig 1B). Next-generation sequence analysis of *k204* and *k207* identified mutations in *emb-9*, which encodes the α1 subunit of collagen IV. Both mutations were amino acid substitutions in the C-terminal NC domain. We generated plasmids carrying these mutant alleles of *emb-9* and introduced them into *mig-17* mutants. The extrachromosomal arrays containing these plasmids partially rescued the gonadal phenotype of *mig-17* mutants (Fig 1B), indicating that *emb-9(k204)* and *emb-9(k207)* mutations are causative for *mig-17* suppression.

We used EMS mutagenesis to isolate suppressors of *gon-1(e1254)*, a strong loss-of-function allele with a nonsense mutation in the C-terminal domain, which contains thrombospondin type 1 motifs (S2 Fig). Although *gon-1(e1254)* homozygotes are sterile, the transgenic strain *gon-1(e1254); tkEx370[gon-1 fosmid, rol-6(su1006), sur-5::GFP]*, which carries an extrachromosomal array that consists of multiple copies of the wild-type *gon-1* fosmid (WRM0622dB04), mutant *rol-6(1006)* plasmid and s*ur-5::GFP* plasmid, does proliferate as a homozygote. *rol-6(su1006)* and *sur-5::GFP* are marker plasmids that result in the roller movement phenotype and GFP expression in all somatic nuclei, respectively. We isolated non-roller and GFP^{-} fertile animals from the

F_2 or F_3 generation of transgenic animals treated with EMS (S3 Fig). One of the two *gon-1* suppressors, *tk101*, acted as a dominant suppressor of *gon-1(e1254)* and was genetically mapped to the right end of LG X. *tk101*was a recessive suppressor for the *gon-1(q518)* null allele (Fig 1C). Next-generation sequence analysis revealed an amino acid substitution in the N-terminal region of the triple helical domain of *let-2*, which encodes the α2 subunit of collagen IV. The extrachromosomal array containing this *let-2* mutant plasmid partially rescued the gonadal phenotype of *gon-1(e1254)* (Fig 1C), indicating that *let-2(tk101)* is the causative mutation for *gon-1* suppression.

Swapping experiments for *mig-17* and *gon-1* suppressors or enhancers

Thus far, our genetic screening had identified various mutant alleles in *let-2* and *fbl-1* that act as suppressors of *mig-17* [11, 12] and in *fbl-1* that act as a suppressor of *gon-1* [14], among which the suppressor mutant alleles differed between *mig-17* and *gon-1*. We also previously showed that loss-of-function mutations *emb-9(g34* and *g23cg46)* and *let-2(g25* and *b246)* act as suppressors of *mig-17* [12] and that *emb-9(tk75)*, which was originally isolated as a suppressor of *fbl-1(tk45)*, acts as an enhancer of *gon-1* [14]. *emb-9(g34* and *g23cg46)* also enhance *gon-1* [14]. In this study, we identified novel suppressors *let-2(tk101)* for *gon-1* and *emb-9(k204* and *k207)* for *mig-17* (Fig 2). These

198 results imply that MIG-17 and GON-1 ADAMTS proteases functionally interact with
199 the same BM proteins collagen IV α1 and α2 subunits and fibulin-1.
200
201 **Fig 2. Suppressor and enhancer mutations for *gon-1* and *mig-17*, and summary for**
202 **swapping experiments of suppressors and enhancers. A.** *fbl-1*, *emb-9* and *let-2*
203 alleles that suppress or enhance the gonadal defects of *gon-1(e1254)* or *mig-17(k174)*.
204 **B.** Locations of mutations in FBL-1C, EMB-9A and LET-2A proteins. The mutation
205 sites are shown by arrowheads (amino acid substitutions) or bidirectional arrows
206 (deletions). Both *fbl-1(tk45)* and *emb-9(g23cg46)* deletions are potential null alleles, as
207 they are expected to introduce termination codons shortly after the deleted region [11,
208 17]. **C.** Summary of effects of *fbl-1*, *emb-9* and *let-2* alleles on *mig-17(k174)* and *gon-*
209 *1(e1254)* mutants. S and E represent suppression and enhancement, respectively.
210
211 To understand the roles shared by these two proteases, we examined how the
212 suppressors of *mig-17* affect *gon-1* and how the suppressors and enhancers of *gon-1*
213 affect *mig-17* gonadal defects. We examined all the combinations of double mutants.
214 The representative phenotypes exhibited by these double mutants are shown in Fig 3,
215 and their phenotypic penetrance scored at the young adult stage is shown in Fig 4 and

Fig 5. In *mig-17(k174)* animals and in double mutants containing *mig-17(k174)*, suppression was assessed by whether the U-shaped gonad was formed as in the wild type. In *gon-1(e1254)* animals and in the double mutants containing *gon-1(e1254)*, suppression was assessed by whether the gonad arms reached the dorsal muscle.

Fig 3. Representative Nomarski images of young adult hermaphrodite gonads of wild-type, *gon-1(e1254)*, *mig-17(k174)* and double-mutant animals analyzed in this study. The gonad morphology is shown by dashed arrows. Anterior is to the left, dorsal up. Arrowheads point to the vulva. Bar: 20 μm.

Fig 4. Percentage of DTC migration defects in *mig-17(k174)* mutants in the presence of *fbl-1*, *emb-9* and *let-2* alleles. $n = 60$ for each experiment. *P*-values from Fisher's exact test comparing the double mutants with *mig-17(k174)* animals: $^{**}P < 0.01$; $^{*}P < 0.05$; NS, not significant.

Fig 5. Percentage of gonad arms that failed to reach the dorsal muscle of *gon-1(e1254)* mutants in the presence of *fbl-1*, *emb-9* and *let-2* alleles. $n = 60$ for each experiment. *P*-values from Fisher's exact test comparing the double mutants with *gon-*

234 *1(e1254)* animals: $**P < 0.01$; $*P < 0.05$; NS, not significant.

235

236 For the *fbl-1* alleles, the *k201* mutation suppressed both *mig-17* and *gon-1*.
237 Although *tk45* suppressed *gon-1*, it rather enhanced *mig-17*. For the *emb-9* alleles,
238 although *g34* and *g23cg46/+* suppressed *mig-17*, they both enhanced *gon-1*. *k204* and
239 *k207* suppressed *mig-17* strongly, whereas they suppressed *gon-1* somewhat weakly.
240 *tk75* acted as a strong enhancer for both *mig-17* and *gon-1*. For the *let-2* alleles,
241 although *g25* and *b246* suppressed *mig-17*, they both enhanced *gon-1*. *tk101*, *k196* and
242 *k193* suppressed both *mig-17* and *gon-1*. These data are summarized in Fig 2C. Because
243 *gon-1* mutants are 100% sterile, we also analyzed fertility in the double mutants (S4
244 Fig). We found that among *fbl-1*, *emb-9* and *let-2*, some alleles suppressed or enhanced
245 both *mig-17* and *gon-1*, whereas others affected *mig-17* and *gon-1* differentially. In the
246 latter case, the alleles that suppressed *mig-17* or *gon-1* rather enhanced *gon-1* or *mig-17*,
247 respectively. These results suggested that the former suppressor alleles suppress the
248 common functional defects in *mig-17* and *gon-1*, whereas the latter alleles suppress
249 gene-specific defects in either *mig-17* or *gon-1*.

250 Three mutations found in EMB-9 (*k204*, *k207* and *tk75*) and one in LET-2 (*k193*)
251 were localized to the C-terminal NC1 domain of these collagen IV molecules. Using

252 SWISS-MODEL, we deduced the three-dimensional structures of the NC1 domains of
253 EMB-9 and LET-2 based on the crystal structures of bovine collagen IV NC1 domains
254 [24] (Fig 6). We found that three amino acid substitutions in EMB-9, which are
255 separated from one another in the primary sequence, were closely apposed in the three-
256 dimensional structure. In the type IV collagen meshwork, triple-helical collagen
257 molecules connect to one another through NC1-NC1 domain interactions. EMB-9(*k207*
258 and *tk75*) mutations were localized to the NC1-NC1 interface regions, and EMB-
259 9(*k204*) was close to these interface regions, suggesting that these amino acid
260 substitutions may affect physical interactions between two NC1 trimers. However,
261 because these mutants were able to proliferate as homozygotes, their mutant collagen
262 molecules were most likely successfully assembled into the functional network in the
263 BM. It is interesting that the amino acid substitutions EMB-9(*k204* and *k207*), which
264 strongly suppressed *gon-1* and *mig-17*, and EMB-9(*tk75*), which strongly enhanced
265 *gon-1* and *mig-17*, were closely localized in the three-dimensional structure.
266
267 **Fig 6. Predicted three-dimensional structures of NC1 domains of *C. elegans* type**
268 **IV collagen subunits EMB-9 and LET-2.** The segments corresponding to the interface
269 region of two NC1 trimers are shown in magenta. The mutated amino acids in the *k204*,

k207, *tk75* and *k193* mutations are highlighted each one in a different color.

Collagen IV accumulation in the DTC BM

Based on an immunohistochemical analysis, we previously reported that the reduced accumulation of collagen IV in the gonadal BM in animals with *fbl-1(tk45)*, a null mutation, can be compensated by *gon-1(e1254)* [14]. To examine the amount of collagen IV accumulation in the BM quantitatively, we used a functional *emb-9::mCherry* fusion reporter [18]. Third larval stage animals in which their DTCs were at or shortly beyond the first turn were selected, and the fluorescence intensity of the BM surrounding the DTCs was measured (Fig 7A-C). Among the six single mutants examined, we observed that the intensity was slightly higher in *fb-1(tk45)*, significantly lower in *let-2(k196)* and significantly higher in *gon-1(e1254)* as compared with wild type. When combined with *fbl-1(k201* and *tk45)* or *let-2(k196* and *g25)* mutations, the level of EMB-9-mCherry accumulation in *mig-17* mutants was not affected except for the case of *let-2(k196)*, in which a slightly lower accumulation was observed (Fig 7B). Because the three mutations *fbl-1(k201)*, *let-2(k196)* and *let-2(g25)* suppressed *mig-17* but *fbl-1(tk45)* did not, the levels of EMB-9-mCherry accumulation were not correlated with *mig-17* suppression. We then combined *fbl-1(k201* and *tk45)* or *let-2(k196* and

288 *g25)* mutations with *gon-1*. We observed that the levels of EMB-9-mCherry
289 accumulation in *fbl-1(k201)*, *fbl-1(tk45)* and *let-2(k196)*, all of which suppress *gon-1*,
290 were significantly lower than that of the *gon-1* single mutants, whereas the level was not
291 affected in *let-2(g25)*, which enhances *gon-1* (Fig 7C). Thus, it is possible that the
292 reduction in EMB-9-mCherry accumulation is indicative of *gon-1* suppression.
293
294 **Fig 7. Accumulation of emb-9-mCherry in the BM. A.** Representative images of
295 optical sections of the gonadal tip shortly after the first turn of the DTCs in wild-type,
296 *mig-17(k174)* and *gon-1(e1254)* animals expressing EMB-9-mCherry. Arrowheads
297 point to DTCs. The right panel illustrates the gonadal BM (brown). The fluorescence
298 intensity of the DTC BM was quantified by averaging the peak values along three lines
299 (green) that cross the DTC BM (see Materials and methods). **B., C.** Box-and-whisker
300 plot of the fluorescence intensity of EMB-9-mCherry in the DTC BM in animals with
301 wild-type and mutant *fbl-1* and *let-2* alleles and with those mutant alleles in
302 combination with *mig-17(k174)* (B) or *gon-1(e1254)* (C); $n = 20$. Boxplots indicate the
303 median and the interquartile range. Whiskers extend to the minimum and maximum
304 values within 1.5 times the interquartile range. Points indicate outliers. *P*-values from
305 Student's t-test are indicated: $**P < 0.01$; $*P < 0.05$; NS, not significant.

Discussion

In the present study, we isolated novel suppressor mutations of gonadal defects related to *mig-17* and *gon-1* mutants. We identified alleles of *emb-9* as *mig-17* suppressors and an allele of *let-2* as a *gon-1* suppressor for the first time. We found that some of the *emb-9 (collagen IV a1)*, *let-2 (collagen IV a2)* and *fbl-1* (*fibulin-1*) mutations suppressed both *gon-1* and *mig-17*, whereas others suppressed only *gon-1* or *mig-17*. These results suggest that *gon-1* and *mig-17* have their specific functions as well as functions in common that relate to gonad formation. Probably, the loss of the gene-specific functions is the cause of the very different phenotypes of the *gon-1* and *mig-17* mutants.

The *fbl-1(tk45)* null mutation suppressed *gon-1* but enhanced *mig-17*. The *gon-1* suppression is likely to be due to the reduction of collagen levels in the late larval stages that results from loss of *fbl-1* activity [14], although the collagen levels were not reduced in the mid-L3 stage when the DTCs make their first turn (Fig 7C). FBL-1C acts downstream of MIG-17 to recruit NID-1/nidogen-1 to regulate directed DTC migration [12]. Thus, *mig-17* is enhanced probably because of the reduction of NID-1 in the DTC BM. In *mig-17* mutants, the DTCs do not migrate along their normal U-shaped route

because they often detach from the body wall (their normal migratory substratum) and mis-attach to the intestine [8]. Therefore, NID-1 is likely to be required for appropriate adhesiveness between the DTC and body wall BMs. The *fbl-1(k201)* gain-of-function mutation suppressed both *mig-17* and *gon-1*. *fbl-1(k201)* suppressed the collagen accumulation in *gon-1*, as did *fbl-1(tk45)*, but *fbl-1(k201)* is fully fertile on its own, unlike *fbl-1(tk45)* (S3 Fig). Therefore, it is possible that the *fbl-1(k201)* mutation may partially compromise the ability of FBL-1C to maintain collagen IV without affecting its ability to recruit NID-1.

The gain-of-function mutations of collagen IV *emb-9(k204, k207)* and *let-2(tk101, k196* and *k193)* were potent suppressors of *mig-17* and *gon-1*. We found that the BM collagen levels in *let-2(k196)* were significantly decreased and that *let-2(k196)* suppressed the dramatic increase in collagen accumulation in *gon-1* animals. Although we did not examine the other gain-of-function collagen mutations, it is possible that the levels of BM collagen are similarly affected. In contrast, the gain-of-function mutation *emb-9(tk75)* enhanced both *mig-17* and *gon-1*. We previously showed that the levels of BM collagen in animals expressing the mutant EMB-9(*tk75*) α1 subunit can be maintained in the absence of FBL-1, which is otherwise required for the maintenance of BM collagen levels [14]. Therefore, it is likely that too much accumulation of collagen

342 in the BM could be causative for both the *mig-17* and *gon-1* mutant phenotypes.
343 Although we could not detect over-accumulation of collagen in the *mig-17* mutant, this
344 could be because of the insufficient sensitivity of our assay condition.
345 This model is not, however, consistent with the fact that the loss-of-function
346 mutations of collagen IV, *emb-9(g34* and *g23cg46/+)* and *let-2(g25* and *b246)*, which
347 conceivably reduce the levels of BM collagen, all acted as enhancers of *gon-1* even
348 though they acted as suppressors of *mig-17*. The loss-of-function *emb-9(xd51)* mutation
349 also enhances *gon-1* in the presynaptic bouton overgrowth phenotype [25]. In contrast,
350 *emb-9(g34)* and *emb-9(b189)* can suppress the synaptic defect of *gon-1* when *emb-9;*
351 *gon-1* double mutants are shifted up from 16 to 25°C after completion of embryogenesis
352 [26]. In this case, it is possible that collagen IV containing the temperature-sensitive
353 mutant proteins EMB-9(*g34*) and EMB-9(*b189*) form intracellular aggregates and thus
354 are not secreted [16], and therefore the BM accumulation of collagen could be
355 considerably decreased. Our analysis using the EMB-9-mCherry reporter revealed that
356 the collagen levels of *let-2(g25); gon-1* or *let-2(g25); mig-17* double mutants were not
357 lowered relative to the respective *gon-1* or *mig-17* single mutant (Fig 7B, C). It might be
358 possible that a subtle reduction in collagen accumulation is sufficient for amelioration
359 of BM physiology in *mig-17* mutants but instead worsens that in *gon-1* mutants. The

360 slight collagen reduction may promote NID-1 accumulation in the BM and suppress the
361 *mig-17* gonadal defect.

362 Why is *gon-1* enhanced by collagen IV loss-of-function mutations? This
363 seemingly contradictory phenomenon may be related to the dual function of GON-1. In
364 addition to its predicted extracellular protease activity, GON-1 functions in the
365 endoplasmic reticulum to transport secreted or membrane proteins from the
366 endoplasmic reticulum to the Golgi. This transport activity is dependent on the C-
367 terminal GON domain but is independent of protease activity [27]. For example, cell
368 surface expression of the integrin receptors that are required for cell migration may be
369 reduced and, therefore, the DTC migration activity in *gon-1* mutants may be weakened.
370 Because the remodeling of the BM is coupled with epithelial cell migration [28, 29],
371 reduced migration of DTCs could also lead to downregulation of BM remodeling,
372 resulting in thick accumulation of collagen, which can further block DTC migration.
373 Remodeling of the BM is likely to be mediated by the GON-1 protease activity.

374 We previously showed that a reduction in collagen IV lowers PAT-3/β-integrin
375 expression in DTCs [14]. At the early second larval stage, the fluorescence levels of
376 EMB-9-mCherry in *gon-1* mutants were closer to those in the wild type (K.N.,
377 unpublished). Thus, it might be possible that when combined with loss-of-function

collagen IV mutants, the reduced collagen levels may further impair integrin expression in DTCs of *gon-1* animals in the second larval or younger stages. This might be the reason for the enhancement of the *gon-1* phenotype in the presence of collagen IV loss-of-function mutations.

It is unclear why the gain-of-function collagen IV mutation *let-2(k196)* did not enhance *gon-1*, as did *let-2(g25)*, even though *let-2(k196)* also reduced collagen accumulation. We speculate that GON-1 is the major enzyme responsible for turnover of BM collagen IV and that the mutant LET(*k196*) protein may confer the property by which the collagen IV meshwork is turned over quickly as compared with the wild-type meshwork even with the weakened activity of GON-1(*e1254*) mutant enzyme. If this is the case, the collagen meshwork containing EMB-9(*tk75*) may have gained a slower turnover rate.

Our observations suggest that both MIG-17 and GON-1 function to reduce collagen IV in the BM**.** Although this is consistent with the idea that collagen IV is the direct substrate of these enzymes, we still do not have evidence of this interaction. Future biochemical analysis is thus needed to determine the substrates. In addition, molecular structural analysis of interactions among these ADAMTS proteases and the BM molecules should shed light on the detailed mechanism of BM remodeling during

396 organogenesis.

397

398 ## Acknowledgments

399 We thank Noriko Nakagawa and Nami Okahashi for technical assistance. Some
400 nematode strains used in this work were provided by the Caenorhabditis Genetics
401 Center, which is funded by the National Institutes of Health National Center for
402 Research Resources. This work was supported by a Grant-in-Aid for Scientific
403 Research on Innovative Areas by Ministry of Education, Culture, Sports, Science and
404 Technology to KN (22111005) and by the Naito Grant for the advancement of natural
405 science to KN.

406

407 ## References

408 1. Apte SS. A disintegrin-like and metalloprotease (reprolysin-type) with
409 thrombospondin type 1 motif (ADAMTS) superfamily: functions and mechanisms. J Biol
410 Chem. 2009;284(46):31493-7. doi: 10.1074/jbc.R109.052340. PubMed PMID: 19734141;
411 PubMed Central PMCID: PMCPMC2797218.
412 2. Mead TJ, Apte SS. ADAMTS proteins in human disorders. Matrix Biol. 2018;71-
413 72:225-39. doi: 10.1016/j.matbio.2018.06.002. PubMed PMID: 29885460; PubMed Central
414 PMCID: PMCPMC6146047.
415 3. Kelwick R, Desanlis I, Wheeler GN, Edwards DR. The ADAMTS (A Disintegrin
416 and Metalloproteinase with Thrombospondin motifs) family. Genome Biol. 2015;16:113. doi:
417 10.1186/s13059-015-0676-3. PubMed PMID: 26025392; PubMed Central PMCID:
418 PMCPMC4448532.
419 4. McCulloch DR, Nelson CM, Dixon LJ, Silver DL, Wylie JD, Lindner V, et al.

ADAMTS metalloproteases generate active versican fragments that regulate interdigital web regression. Dev Cell. 2009;17(5):687-98. doi: 10.1016/j.devcel.2009.09.008. PubMed PMID: 19922873; PubMed Central PMCID: PMCPMC2780442.

5. Nandadasa S, Kraft CM, Wang LW, O'Donnell A, Patel R, Gee HY, et al. Secreted metalloproteases ADAMTS9 and ADAMTS20 have a non-canonical role in ciliary vesicle growth during ciliogenesis. Nat Commun. 2019;10(1):953. doi: 10.1038/s41467-019-08520-7. PubMed PMID: 30814516; PubMed Central PMCID: PMCPMC6393521.

6. Stupka N, Kintakas C, White JD, Fraser FW, Hanciu M, Aramaki-Hattori N, et al. Versican processing by a disintegrin-like and metalloproteinase domain with thrombospondin-1 repeats proteinases-5 and -15 facilitates myoblast fusion. J Biol Chem. 2013;288(3):1907-17. doi: 10.1074/jbc.M112.429647. PubMed PMID: 23233679; PubMed Central PMCID: PMCPMC3548499.

7. Blelloch R, Kimble J. Control of organ shape by a secreted metalloprotease in the nematode *Caenorhabditis elegans*. Nature. 1999;399(6736):586-90. doi: 10.1038/21196. PubMed PMID: 10376599.

8. Nishiwaki K, Hisamoto N, Matsumoto K. A metalloprotease disintegrin that controls cell migration in *Caenorhabditis elegans*. Science. 2000;288(5474):2205-8. doi: 10.1126/science.288.5474.2205. PubMed PMID: 10864868.

9. Ihara S, Nishiwaki K. Prodomain-dependent tissue targeting of an ADAMTS protease controls cell migration in *Caenorhabditis elegans*. EMBO J. 2007;26(11):2607-20. doi: 10.1038/sj.emboj.7601718. PubMed PMID: 17491590; PubMed Central PMCID: PMCPMC1888677.

10. Keeley DP, Hastie E, Jayadev R, Kelley LC, Chi Q, Payne SG, et al. Comprehensive Endogenous Tagging of Basement Membrane Components Reveals Dynamic Movement within the Matrix Scaffolding. Dev Cell. 2020;54(1):60-74 e7. doi: 10.1016/j.devcel.2020.05.022. PubMed PMID: 32585132; PubMed Central PMCID: PMCPMC7394237.

11. Kubota Y, Kuroki R, Nishiwaki K. A fibulin-1 homolog interacts with an ADAM protease that controls cell migration in *C. elegans*. Curr Biol. 2004;14(22):2011-8. doi: 10.1016/j.cub.2004.10.047. PubMed PMID: 15556863.

12. Kubota Y, Ohkura K, Tamai KK, Nagata K, Nishiwaki K. MIG-17/ADAMTS controls cell migration by recruiting nidogen to the basement membrane in *C. elegans*. Proc Natl Acad Sci U S A. 2008;105(52):20804-9. doi: 10.1073/pnas.0804055106. PubMed PMID: 19104038; PubMed Central PMCID: PMCPMC2634947.

13. Hesselson D, Newman C, Kim KW, Kimble J. GON-1 and fibulin have antagonistic roles in control of organ shape. Curr Biol. 2004;14(22):2005-10. doi:

10.1016/j.cub.2004.11.006. PubMed PMID: 15556862.

14. Kubota Y, Nagata K, Sugimoto A, Nishiwaki K. Tissue architecture in the *Caenorhabditis elegans* gonad depends on interactions among fibulin-1, type IV collagen and the ADAMTS extracellular protease. Genetics. 2012;190(4):1379-88. doi: 10.1534/genetics.111.133173. PubMed PMID: 22298704; PubMed Central PMCID: PMCPMC3316650.

15. Brenner S. The genetics of *Caenorhabditis elegans*. Genetics. 1974;77(1):71-94. PubMed PMID: 4366476; PubMed Central PMCID: PMCPMC1213120.

16. Gupta MC, Graham PL, Kramer JM. Characterization of α1(IV) collagen mutations in *Caenorhabditis elegans* and the effects of alpha1 and α2(IV) mutations on type IV collagen distribution. J Cell Biol. 1997;137(5):1185-96. doi: 10.1083/jcb.137.5.1185. PubMed PMID: 9166417; PubMed Central PMCID: PMCPMC2136222.

17. Sibley MH, Graham PL, von Mende N, Kramer JM. Mutations in the alpha 2(IV) basement membrane collagen gene of *Caenorhabditis elegans* produce phenotypes of differing severities. EMBO J. 1994;13(14):3278-85. PubMed PMID: 8045258; PubMed Central PMCID: PMCPMC395224.

18. Kim HS, Kitano Y, Mori M, Takano T, Harbaugh TE, Mizutani K, et al. The novel secreted factor MIG-18 acts with MIG-17/ADAMTS to control cell migration in *Caenorhabditis elegans*. Genetics. 2014;196(2):471-9. doi: 10.1534/genetics.113.157685. PubMed PMID: 24318535; PubMed Central PMCID: PMCPMC3914620.

19. Wicks SR, Yeh RT, Gish WR, Waterston RH, Plasterk RH. Rapid gene mapping in Caenorhabditis elegans using a high density polymorphism map. Nat Genet. 2001;28(2):160-4. doi: 10.1038/88878. PubMed PMID: 11381264.

20. Nishiwaki K. Mutations affecting symmetrical migration of distal tip cells in *Caenorhabditis elegans*. Genetics. 1999;152(3):985-97. PubMed PMID: 10388818; PubMed Central PMCID: PMCPMC1460665.

21. Mello CC, Kramer JM, Stinchcomb D, Ambros V. Efficient gene transfer in *C.elegans*: extrachromosomal maintenance and integration of transforming sequences. EMBO J. 1991;10(12):3959-70. PubMed PMID: 1935914; PubMed Central PMCID: PMCPMC453137.

22. Maduro M, Pilgrim D. Identification and cloning of unc-119, a gene expressed in the *Caenorhabditis elegans* nervous system. Genetics. 1995;141(3):977-88. PubMed PMID: 8582641; PubMed Central PMCID: PMCPMC1206859.

23. Yochem J, Gu T, Han M. A new marker for mosaic analysis in *Caenorhabditis elegans* indicates a fusion between hyp6 and hyp7, two major components of the hypodermis. Genetics. 1998;149(3):1323-34. PubMed PMID: 9649523; PubMed Central

PMCID: PMCPMC1460238.

24. Sundaramoorthy M, Meiyappan M, Todd P, Hudson BG. Crystal structure of NC1 domains. Structural basis for type IV collagen assembly in basement membranes. J Biol Chem. 2002;277(34):31142-53. doi: 10.1074/jbc.M201740200. PubMed PMID: 11970952.

25. Qin J, Liang J, Ding M. Perlecan antagonizes collagen IV and ADAMTS9/GON-1 in restricting the growth of presynaptic boutons. J Neurosci. 2014;34(31):10311-24. doi: 10.1523/JNEUROSCI.5128-13.2014. PubMed PMID: 25080592; PubMed Central PMCID: PMCPMC6608278.

26. Kurshan PT, Phan AQ, Wang GJ, Crane MM, Lu H, Shen K. Regulation of synaptic extracellular matrix composition is critical for proper synapse morphology. J Neurosci. 2014;34(38):12678-89. doi: 10.1523/JNEUROSCI.1183-14.2014. PubMed PMID: 25232106; PubMed Central PMCID: PMCPMC4166155.

27. Yoshina S, Sakaki K, Yonezumi-Hayashi A, Gengyo-Ando K, Inoue H, Iino Y, et al. Identification of a novel ADAMTS9/GON-1 function for protein transport from the ER to the Golgi. Mol Biol Cell. 2012;23(9):1728-41. doi: 10.1091/mbc.E11-10-0857. PubMed PMID: 22419820; PubMed Central PMCID: PMCPMC3338439.

28. Yamada KM, Collins JW, Cruz Walma DA, Doyle AD, Morales SG, Lu J, et al. Extracellular matrix dynamics in cell migration, invasion and tissue morphogenesis. Int J Exp Pathol. 2019;100(3):144-52. doi: 10.1111/iep.12329. PubMed PMID: 31179622; PubMed Central PMCID: PMCPMC6658910.

29. Morrissey MA, Sherwood DR. An active role for basement membrane assembly and modification in tissue sculpting. J Cell Sci. 2015;128(9):1661-8. doi: 10.1242/jcs.168021. PubMed PMID: 25717004; PubMed Central PMCID: PMCPMC4446735.

Supporting information

S1 Fig. Schematic presentation of gonad formation in the *C. elegans* hermaphrodite. The hermaphrodite U-shaped gonad arms are generated by migration of two DTCs. DTCs are generated at the anterior (A) and posterior (P) ends of the gonad primordium at the first larval stage (L1) and migrate along the anteroposterior axis on the ventral (V) body wall muscle (L2–L3). The DTCs turn dorsally (D) and

522 migrate along the lateral hypodermis (L3). Finally, the DTCs undergo a second turn and
523 migrate along the dorsal body wall muscle to form the symmetrical U-shaped arms
524 (L4).
525
526 **S2 Fig. Structure and mutation sites of GON-1 and MIG-17 proteins.** Domain
527 organization is shown by colored boxes. Mutation sites for *gon-1(q518* and *e1254)* and
528 *mig-17(k174)* are indicated.
529
530 **S3 Fig. Isolation of *gon-1* suppressors.** Gonad arms (arrows) of young adult
531 hermaphrodites are shown. **A., B.** Nomarski images of wild type (A) and *gon-1(e1254)*
532 (B). **C., D.** Nomarski (C) and fluorescence (D) images of a *gon-1(e1254); tkEx370[gon-*
533 *1 fosmid, rol-6(su1006), sur-5::GFP]* young adult hermaphrodite. **E., F.** Nomarski (E)
534 and fluorescence (F) images of a *let-2(k101); gon-1(e1254)* young adult hermaphrodite,
535 which lost the *tkEx370[gon-1 fosmid, rol-6(su1006), sur-5::GFP]* extrachromosomal
536 array.
537
538 **S4 Fig. Percentage of fertile animals.** For each strain, 20 first larval stage
539 hermaphrodites were grown at 20°C, and the number of animals that produced offspring

were counted. Green and red bars represent % fertile and % sterile animals, respectively.

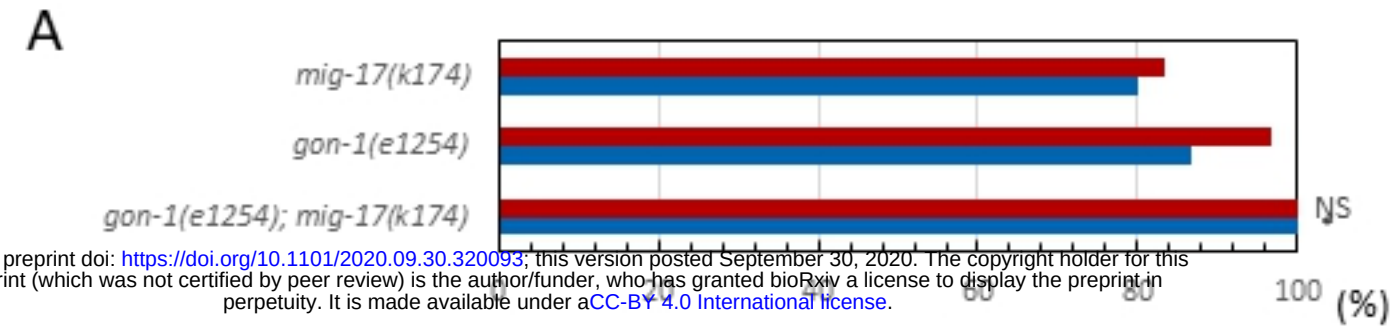

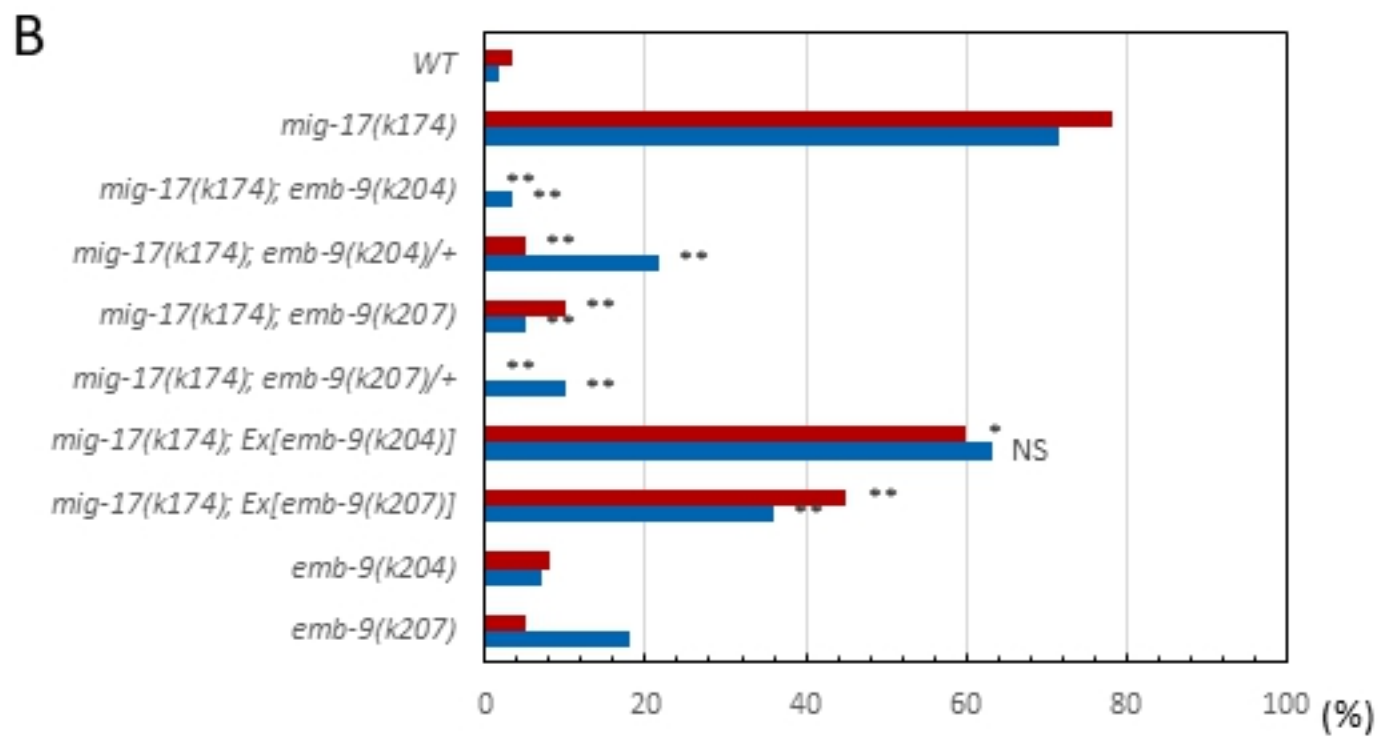

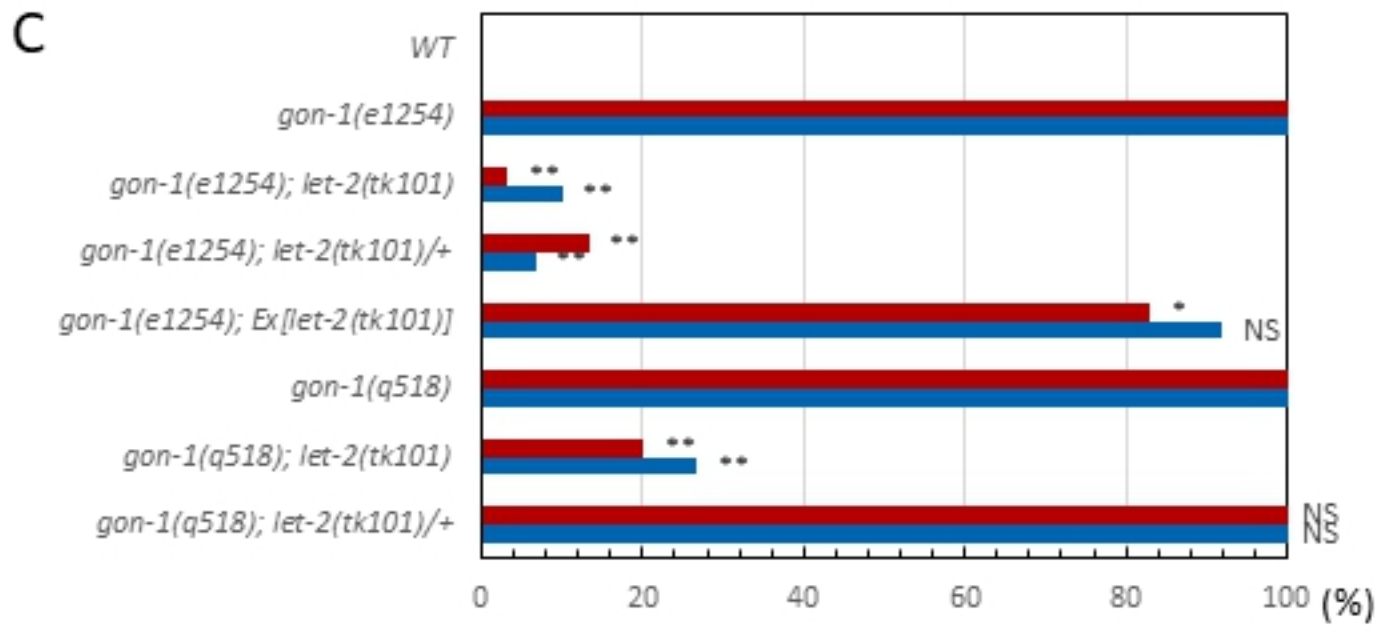

Fig 1

Fig 1

A

	***gon-1* suppressor or enhancer**	***mig-17* suppressor**
fbl-1	*tk45*	*k201*
emb-9	*tk75, g34, g23cg46 (enhancers)*	*g34, g23cg46, k204, k207*
let-2	*tk101*	*g25, b246, k193, k196*

B

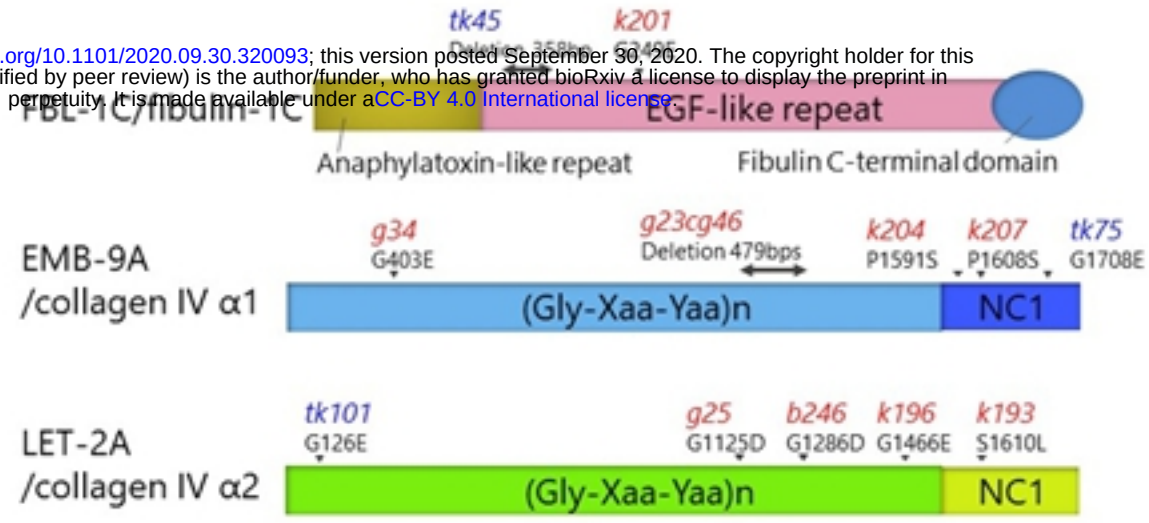

C

	Allele	*mig-17*	*gon-1*
fbl-1	*tk45*	E	S
	k201	S	S
emb-9	*g34*	S	E
	g23cg46/+	S	E
	k204	S	S
	k207	S	S
	tk75	E	E
let-2	*g25*	S	E
	b246	S	E
	tk101	S	S
	k196	S	S
	k193	S	S

Fig 2

Fig 2

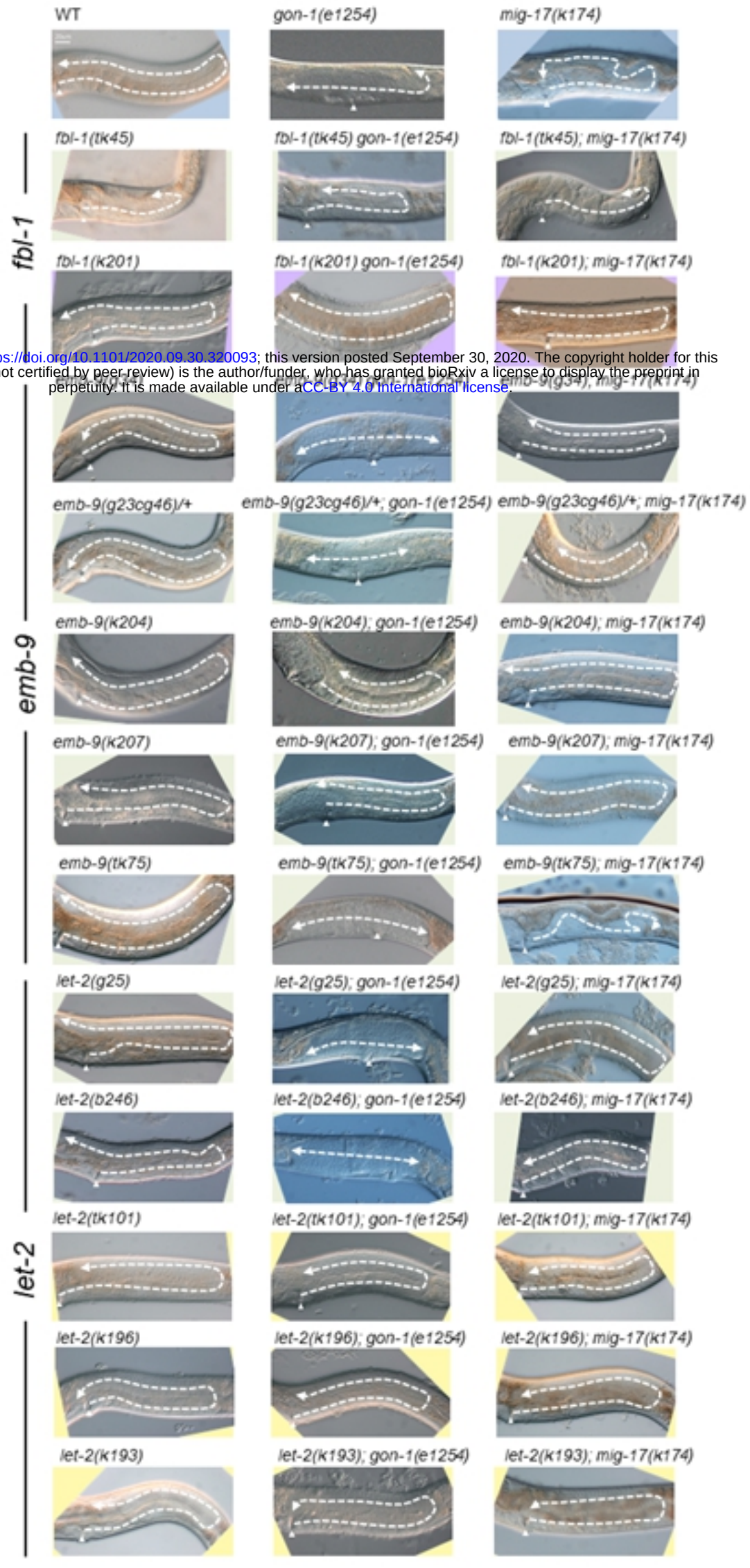

Fig 3

Fig 3

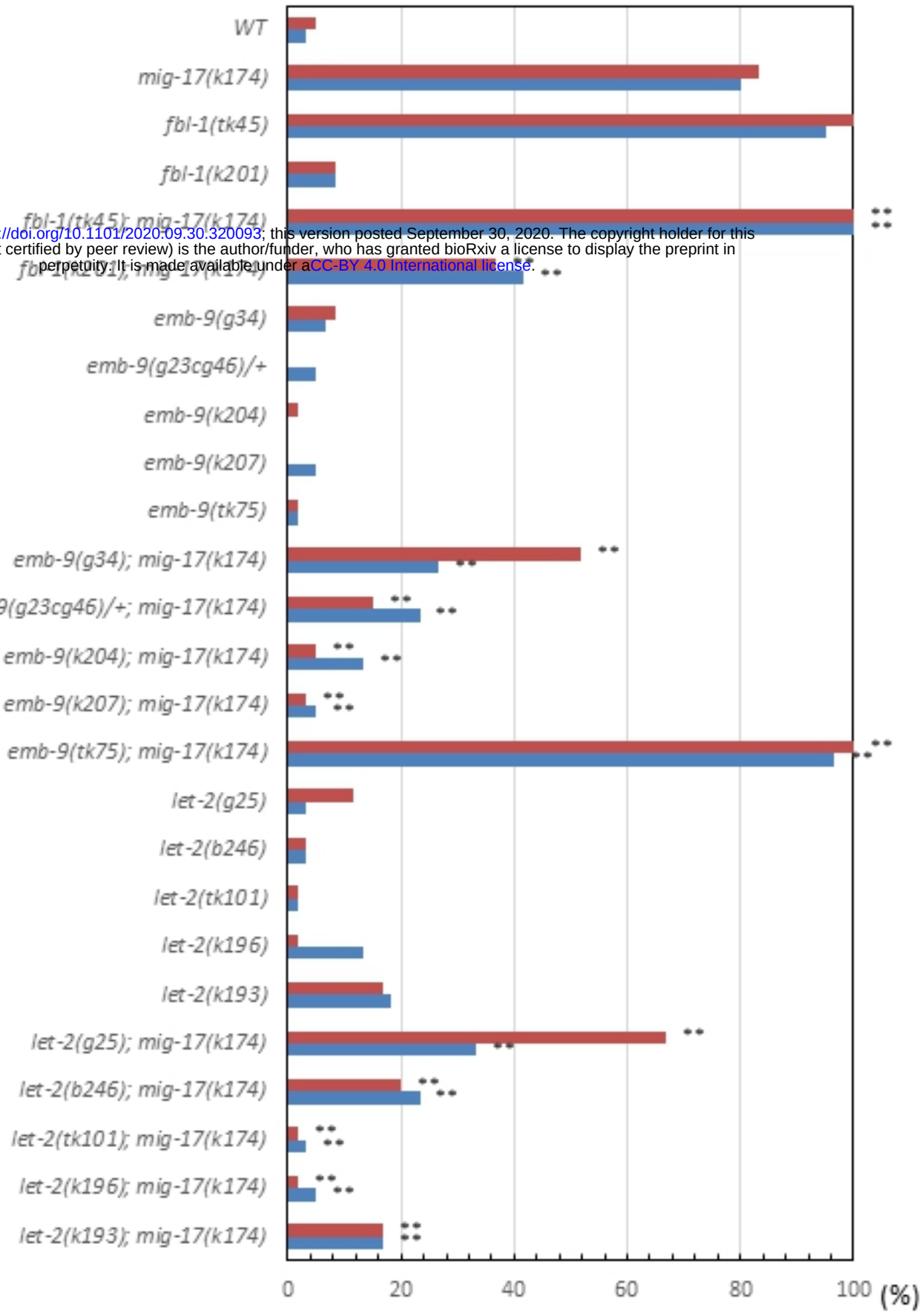

Fig 4

Fig 4

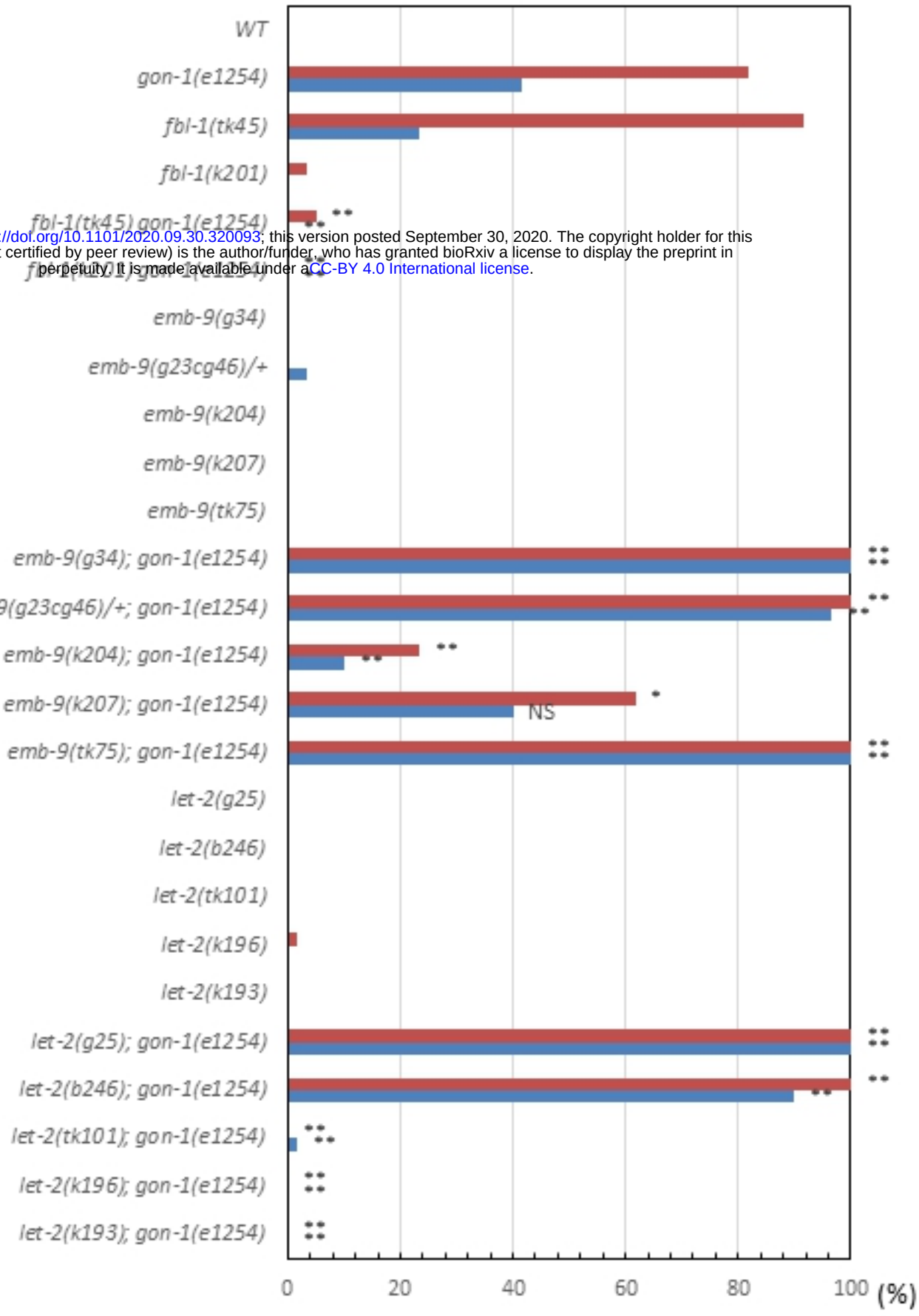

Fig 5

Fig 5

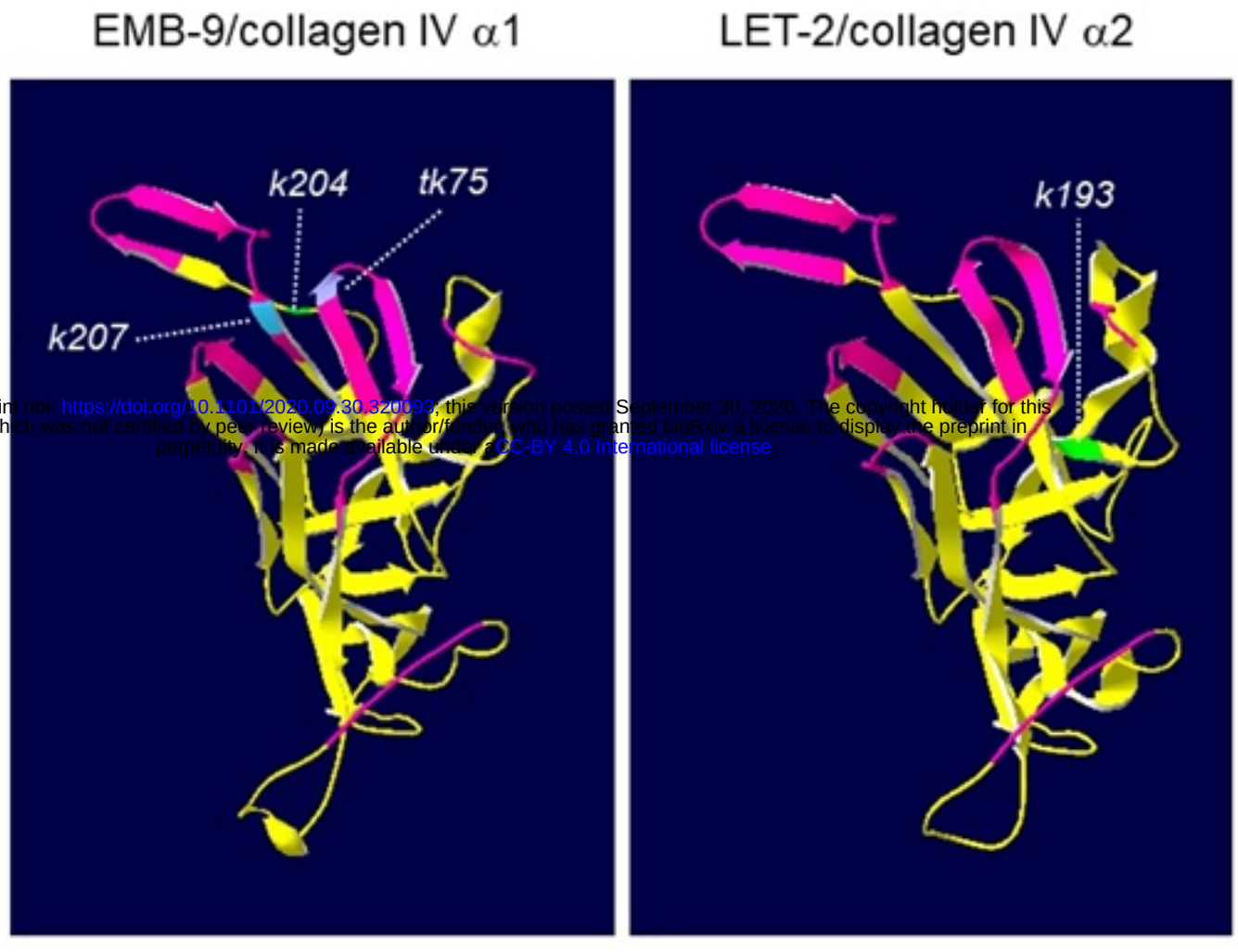

Fig 6

Fig 6

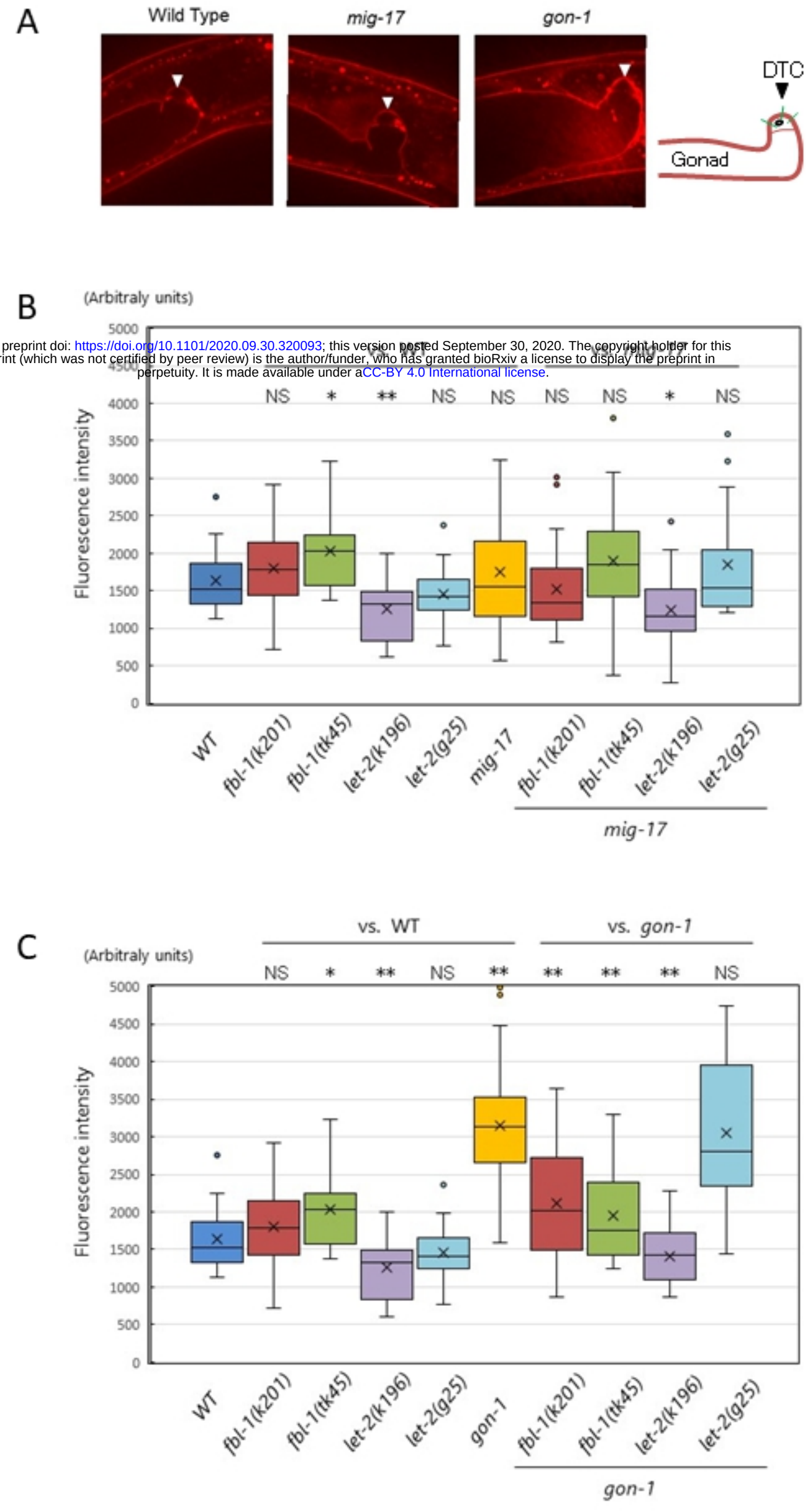

Fig 7

Fig 7